ACS MATERIALS LETTERS

www.acsmaterialsletters.org

Near-Infrared Emission in Organic Cocrystals Based on Twisted-Component Pseudoencapsulation

Tao Li, Bai-Tong Liu, Jia-Chuan Liu, Niharika Ashutosh Sule, Jennifer T. Ou, Jim Y. Huang, Chenxin Ou, Jian-Hua Jia,* and Yuanning Feng*

Cite This: ACS Materials Lett. 2025, 7, 2246−2254

Read Online

ACCESS | Metrics & More | Article Recommendations | Supporting Information

ABSTRACT: **Near-infrared (NIR) fluorescence, prized for deep optical penetration and high spatial resolution, can be achieved in organic cocrystals via donor−acceptor (D−A) charge-transfer (CT) emissions. We have rationally synthesized a series of cocrystals consisting of a twisted tetrachloroperylene dianhydride (TCPDA) as the electron-deficient acceptor, incorporating respectively with three different polycyclic aromatic hydrocarbons—i.e., triphenylene (TP), coronene (Cor), and perylene (Per)—as electron-rich donors. The introduction of a twisted component provides a pseudoencapsulation strategy to achieve fine-tuned control over stoichiometries, solid-state superstructures, and D−A interactions. Fluorescence emission spectra of these three cocrystals cover a wide range of wavelengths up to 861 nm. TP−TCPDA cocrystals with a two-photon absorption band reach into the NIR-II region because of the manipulation of the twisted configuration and noncovalent interactions. The pseudoencapsulation strategy of applying twisted components in cocrystals holds considerable promise for the future design and synthesis of advanced optical materials.**

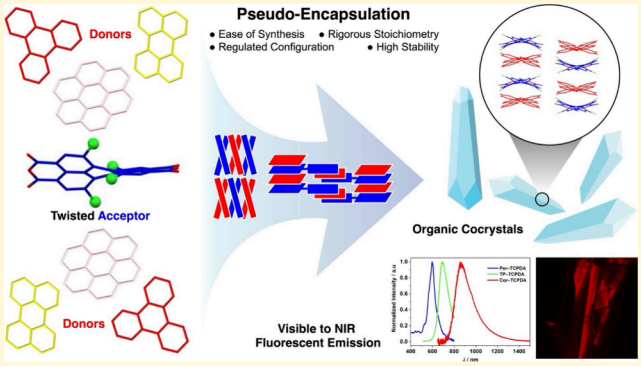

Near-infrared (NIR) light exhibits superior properties including higher optical penetration, lesser photodamage, and lower optical scattering compared to visible (Vis) light.[1−4] Organic NIR emitting materials have broad applications in the fields of bioimaging,[5−7] remote sensing,[8] optical communication/diagnosis,[9] night-vision technologies,[10] and advanced optoelectronics.[11,12] To date, the organic NIR emitters have been constructed mainly by conjugated polymers,[13,14] small molecule dyes,[15−17] and organic noble-metal/rare-earth complexes.[14,18] Correspondingly, immense efforts have been devoted to the design philosophy and synthesis methods for finding the desired organic NIR materials with higher fluorescence efficiency and longer emission wavelengths. For instance, the introduction of (i) excited state intramolecular proton transfer[19] with strong charge-transfer (CT) effect,[20] (ii) extended π-conjugation length,[21] and (iii) tunable molecular stacking modes[22] has led to much success. However, achieving NIR emission wavelengths (λ_{em}) over 700 nm in pure organic fluorescent materials is challenging because of the lack of control strategies.[23−25] An alternative approach for constructing NIR-absorbing materials is to utilize two-photon absorption (2PA), which can convert the excitation wavelengths (λ_{ex}) from the Vis region to the NIR region. Two-photon excited NIR-emitting materials with inherent multifunctionality are ideal candidates for cell imaging,[26−28] photodynamic therapy,[29−32] microfabrication,[33] and optical data storage.[34,35] Compared with Vis (400−700 nm) and NIR-I (700−1000 nm) light imaging, NIR-II (1000−1700 nm) imaging exhibits smaller scattering and absorption coefficients in samples, resulting in higher imaging resolutions and penetration depths.[36] The design of NIR materials suffers[37,38] from complicated and sophisticated fabrication techniques.

Recently, progress has been made in the study of supramolecular assemblies whose main driving forces are noncovalent interactions.[39−45] Donor−acceptor (D−A) systems based on CT interactions have emerged as an attractive class of materials because of their potential applications in

Received: February 10, 2025
Revised: May 9, 2025
Accepted: May 9, 2025
Published: May 15, 2025

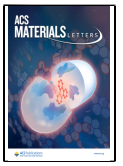

optoelectronic devices,[46,47] field-effect transistors,[48] ferroelectric materials,[49] dynamic photomechanics,[50] and nonlinear optics.[37,38,51] Thanks to well-developed synthetic strategies, the characteristics of organic molecules can be tuned, allowing for the design of various CT systems. Assemblies of D−A systems are complicated and usually affected by multiple factors;[40,48,52,53] therefore, small changes can cause profound defects, leading to unwanted polymorphic crystallization and stoichiometric offsets. In the traditional D−A stacking systems with no encapsulation (Figure 1a, left), because of the slipping along the π-planes, the stability and control of stoichiometry can be limited. In comparison, full encapsulation (Figure 1a, right) typically refers to guest molecules entirely enclosed by macrocyclic hosts[54−56] or organic porous materials.[57−61] These systems provide a well-defined confined environment, leading to stable supramolecular superstructures with controlled host−guest (H−G) interactions and enhanced functional properties. In this research, we introduced a twisted molecule that adopts a nonplanar conformation because of steric hindrance, electronic effects, or intrinsic molecular strain. For instance, *ortho*-substituted polyaromatic compounds exhibit structural distortion caused by the spatial repulsion between substituents. This structural twist plays a crucial role in modulating intermolecular [$\pi\cdots\pi$] stacking, self-assembly behavior, and photoelectric properties. Twisted molecules can regulate configurations and supramolecular interactions with their counterparts, providing a strategy that we coined as pseudoencapsulation (Figure 1a, middle). Compared to traditional full encapsulation, the pseudoencapsulation strategy is capable of controlling stoichiometry, geometry, and selectivity without the requirements of complex compounds, enabling more straightforward synthesis and manipulation.

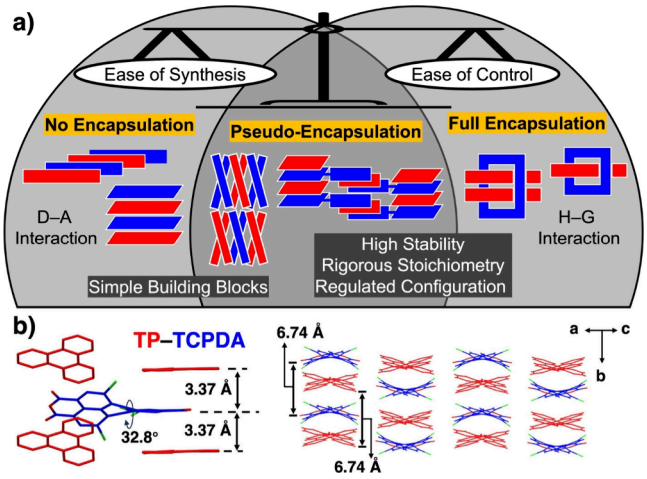

Figure 1. (a) Venn diagram illustrating the superstructures of different encapsulation methods. No encapsulation (left), which relies on donor−acceptor (D−A) and/or [$\pi\cdots\pi$] stacking, has limited stability and control of stoichiometry. Full encapsulation (right) relies on strong host−guest (H−G) interactions, where the guest molecule is fully enclosed by the macrocyclic host or organic porous materials. In contrast, the pseudoencapsulation strategy in this research utilizes molecular twisting to drive restricted stacking via D−A interactions, achieving structural control without external host molecules. (b) Single crystal X-ray diffraction (SC-XRD) superstructure of the TP−TCPDA cocrystal exhibits the twisted configuration in the TCPDA component and D−A stacking arrays along the *b*-axis.

Configurations of twisted components exhibit predictable trends, while the systematic study[62−64] of the pseudoencapsulation strategy for facilitating the photophysical properties of self-assembly is still underdeveloped.

Herein, three cocrystals were synthesized using an electron-deficient 1,6,7,8-tetrachloro-3,4,9,10-perylenetetracarboxylic dianhydride (**TCPDA**) component as the acceptor, combined with three electron-rich polycyclic aromatic hydrocarbons (PAHs)—triphenylene (**TP**), coronene (**Cor**), and perylene (**Per**), respectively—as donors. Solid-state superstructures revealed that all cocrystals have a similar D−A array, utilizing CT between the packing arrays. The pseudoencapsulation strategy involves the construction of a space in the solid state that regulates the intermolecular interactions, resulting in well-aligned superstructures and the rigorous 2:1 (D:A) stoichiometry. Fluorescence emission spectra demonstrate that their λ_{em} values differ for each cocrystal, with values up to 861 nm in **Cor−TCPDA**. Superstructural, computational, and transient absorption (TA) spectroscopic analyses have shown that intermolecular interactions in twisted component-containing cocrystals facilitate the suppression of large-amplitude nuclear motion, leading to efficient NIR emission. This specific stacking mode and spatial segregation that leads to small electron-transfer integral values, as well as the suppression of large amplitude nuclear motion are conducive to achieving a CT state to partial electron transitions and attractive NIR emission. More importantly, CT emissions are achieved by the combination of twisted **TCPDA** and PAHs. The emission properties of these can be modulated rationally over a wide range by the appropriate choice of donors with proper ionization potentials.

One of the cocrystals, **TP−TCPDA**, exhibits notable 2PA in the NIR-II region, which can serve as a powerful tool for uncovering the superstructure−property relationship. This investigation provides insights into the manipulation of photophysical properties in supramolecular systems and sheds light on the possibility of employing twisted components as a strategy to produce multifunctional materials.

The synthetic procedure can be found in the Supporting Information. Thermogravimetric analysis of all of the cocrystals (Figure S1) indicates that weight loss begins after 200 °C, confirming the thermal stability. Solid-state superstructures of **TP−TCPDA**, **Cor−TCPDA**, and **Per−TCPDA** cocrystals (Figures S2−S4) were determined (Table S1) by single-crystal X-ray diffraction (SC-XRD). **TP−TCPDA**, as an example, is shown in Figure 1b. Each **TCPDA** acceptor interacted with two neighboring pairs of **TP** donors at both sides through [$\pi\cdots\pi$] interactions next to dichloronaphthalic anhydride units. Compared to an individual twisted **TCPDA** molecule (Figure S5), which exhibits[46] a torsional angle of 41.8° between two dichloronaphthalic anhydride units, the torsional angle in **TP−TCPDA** cocrystals is 32.8° (Figure S6). Similar behavior was observed in both **Cor−TCPDA** and **Per−TCPDA** cocrystals (Figures S7 and S8), with decreased torsional angles of 34.8° and 35.7°, respectively. The decrease in the twisted angle reflects the impact of the donors on the configuration of **TCPDA**, which facilitates better D−A interactions by promoting the dispersion and separation of guest molecules within the twisted structure, thus preventing aggregation. Three benzenoid rings in the **TP** unit exhibited (Figure S5) a maximum torsional angle of 4.5°, which decreased (Figure S6) to nearly 0° in the **TP−TCPDA** cocrystal. In contrast, both **Cor** and **Per** units had a planar geometry in their individual

https://doi.org/10.1021/acsmaterialslett.5c00275
ACS Materials Lett. 2025, 7, 2246−2254

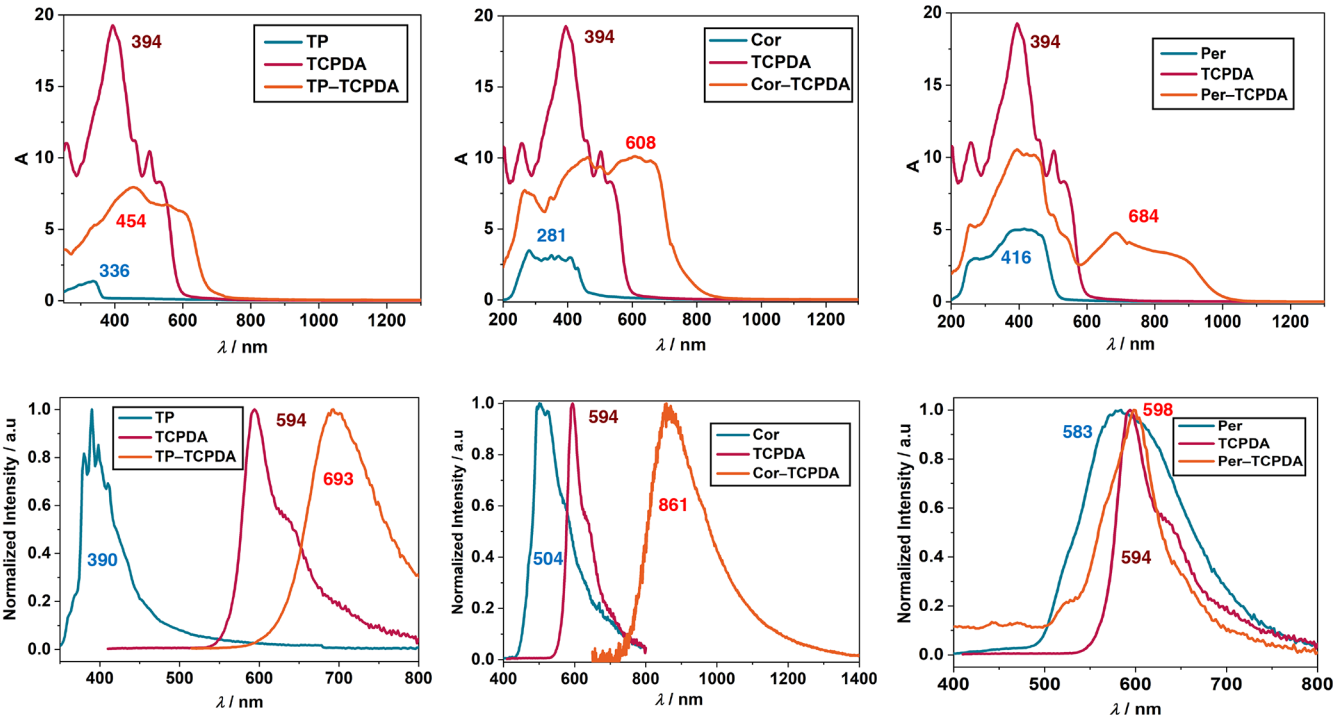

Figure 2. Solid-state UV−Vis−NIR diffuse reflectance (top) and normalized fluorescence (λ_{ex} = 380 nm, bottom) spectra of TP−TCPDA (left), Cor−TCPDA (middle), and Per−TCPDA (right) cocrystals overlaid with each of the components, respectively, at 298 K.

crystals. In each cocrystal, however, the naphtho rings in each PAH donor distort to torsional angles of 2.2° (**Cor−TCPDA**) and 5.2° (**Per−TCPDA**), respectively. **TCPDA** is twisted through its long axis with a torsional angle of 32.8° between two dichloronaphthalic anhydride units. Along the *b*-axis, D and A form alternative layers with a planar-to-planar distance of ∼3.37 Å. In each two-dimensional (2D) layer (Figure S9), each of the two **TP** molecules align in an antiparallel manner, forming a pair that integrates into a mosaic pattern with single-oriented **TCPDA**. A powder XRD experiment was carried out, and its pattern matched (Figures S10−S13) with the simulated multilayer result, proving that the well-organized D−A superstructure was synthesized without defects.

TP−TCPDA, **Cor−TCPDA**, and **Per−TCPDA** cocrystals in the solid-state exhibit dark red, black, and dark green colors, respectively. Using an integrating sphere, solid-state ultraviolet−visible (UV−Vis) absorption spectra of the **TCPDA** crystal exhibited a broad band below 600 nm. All cocrystals exhibited completely different UV−Vis absorption spectra compared to the individual **TP**, **Cor**, and **Per** crystals (Figure 2, top). These changes in absorption spectra can be ascribed to the CT interactions between each donor and twisted **TCPDA** acceptor, further demonstrating the formation based on the pseudoencapsulation strategy. The simulated absorption spectra (Figure S16) of the cocrystals match the experimental absorption spectra, which provide theoretical evidence for the occurrence of CT interactions.

Fluorescence spectra (λ_{ex} = 380 nm) revealed that although three cocrystals exhibit similar superstructures in the solid state, their photophysical behavior depends on the identity of the PAH donor. Individual **TCPDA** crystals exhibited a λ_{em} at 594 nm (Figure 2, bottom), whereas cocrystals that were incorporated with PAH donors covered a broad λ_{em} at 600−1000 nm. The **Per−TCPDA** cocrystal did not display an obvious red-shift in emission (λ_{em} = 598 nm) compared with that of individual **TCPDA**. Both **TP−TCPDA** and **Cor−TCPDA** cocrystals exhibited unusual broadband NIR emissions with large Stokes shifts, peaking at 693 and 861 nm, which can be calculated as 0.94 and 0.60 eV, respectively. These large shifts suggest that the fluorescence emission came from the strongly coupled CT state in a bimolecular D−A system (rather than a single molecule) as a result of significant supramolecular configurational reorganizations in the excited state,[23] which proves the advantage of incorporating twisted components as chromophores for distinct emissions. The unchanged shape and position of these NIR emissions at various λ_{ex} (380 or 400 nm) indicate that these NIR emissions (Figure S14) originate from the relaxations of the same excited states.[65] The relationship between the λ_{em} values of three cocrystals and the ionization potential of the PAH donors is shown in Figures S15. Compared to previous studies,[66,67] the **Per−TCPDA** cocrystal is observed to have unique performance, which will be further investigated in another in-depth research project. Molecular electrostatic potential (ESP) analysis (Figure 3, top) indicates that all PAH donors exhibit high electron richness, whereas the **TCPDA** acceptor in each cocrystal possesses deep π−holes. Each D−A system facilitates strong [$\pi\cdots\pi$] interactions, which exhibit different degrees of overlap between the twisted **TCPDA** acceptor and the relative PAH donors. This discrepancy in overlap is expected to influence the extent of CT between D and A, consequently impacting their respective emissions consequently.

Density functional theory (DFT) calculations exhibit that the lowest unoccupied molecular orbital (LUMO) energy levels of **TP**, **Cor**, and **Per** (Figure S17, top) are significantly higher than that of **TCPDA**, with a more noticeable energy difference compared with the HOMO levels. Similarly, the HOMO energy levels of these three guests (Figure S17,

https://doi.org/10.1021/acsmaterialslett.5c00275
ACS Materials Lett. 2025, 7, 2246−2254

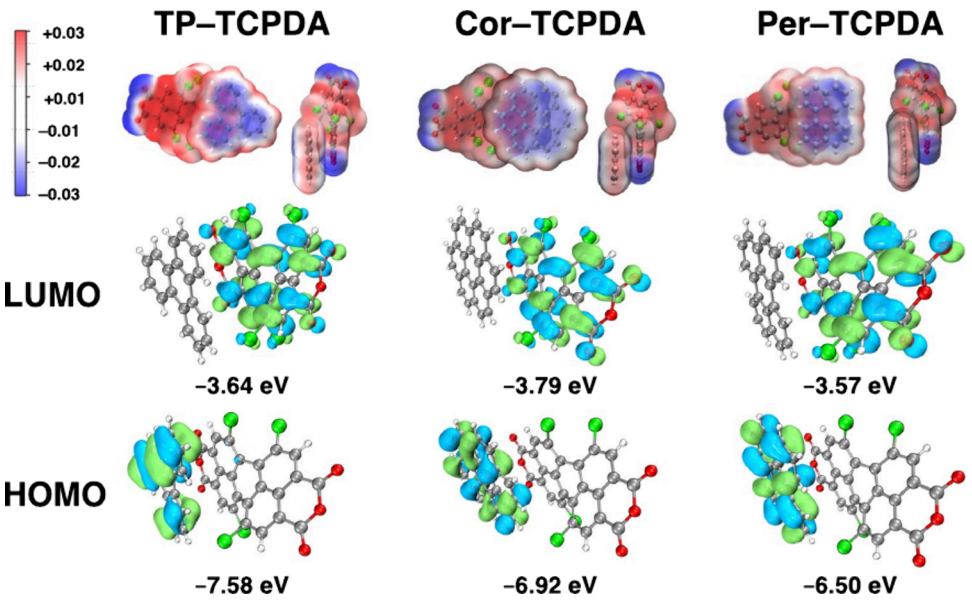

Figure 3. Graphical representations of electrostatic potential (ESP, top) analyses and lowest unoccupied (LUMO, middle) and highest occupied (HOMO, bottom) molecular orbitals of TP−TCPDA (left), Cor−TCPDA (middle), and Per−TCPDA (right) and the corresponding energy gaps, respectively.

bottom) are also higher than those of **TCPDA**, which contributes to the electronic properties of the system. The simulated MO of the cocrystals (Figure 3, bottom) differs from those of individual components, respectively. The differences in the bandgap of cocrystals arose from the change of D−A CT degree. Based on the energy levels in the ground state, the LUMO of **TCPDA** and each HOMO of **TP**, **Cor**, and **Per** exhibit the narrowest bandgaps, which confirms the assignment of D, A, and CT directions. Compared to those of **TP** and **Cor**, the HOMO of **Per** was relatively higher, which matches with the stronger CT interactions in the **Per−TCPDA** cocrystal. This tendency agrees with UV−Vis−NIR absorption spectra (Figure 2, top, and Figure S16). Visualized diagrams demonstrate that the newly formed HOMOs of cocrystals distribute mainly on each PAH donor, whereas LUMOs distribute mainly on the **TCPDA** acceptor in each system, illustrating that CT interactions in the ground state are weak. These results demonstrate that the changes in CT degrees result from variations in supramolecular coconfigurations, hence tuning the electron distributions and photophysical properties of cocrystals.

We carried out the following time-dependent density functional theory (TD-DFT) analysis to investigate the principle to explain the off-path data of the **Per−TCPDA** cocrystal. The TD-DFT calculated absorption spectra of three cocrystals show broadbands in the Vis region, indicating (Figure S18 and Table S3−S5) transitions from HOMO to LUMO. This data confirms the intermolecular CT from D to A in cocrystals. Typical excited transitions—featuring both $D_{HOMO}\rightarrow A_{LUMO}$ and $D_{HOMO-1}\rightarrow$CT—exhibit the bandgap in the IR region. The transfer integral was demonstrated using a D−A stacking dimer as a model. The electron-transfer integral value (ETIV) of **TP−TCPDA**, **Cor−TCPDA**, and **Per−TCPDA** cocrystals is relatively at the same level (0.7618, 0.7490, and 0.7059 eV, respectively), which is larger than that of a common D−A stacking (∼0.300 eV). According to their visualized diagrams (Figure S19, top), the main transition pathways in the three cocrystals all follow the intramolecular CT within the **TCPDA** component, resulting from its nonplanar configuration. The hole-transfer integral value (HTIV) of **Per−TCPDA** (0.7184 eV) is dramatically higher than those of the other two cocrystals (0.0163 and 0.0293 eV, respectively). In their visualized diagrams (Figure S19, bottom), **Per−TCPDA** exhibits an abnormal pattern: instead of all HOMO−1 orbitals being on the PAH donors (such as in both **TP−TCPDA** and **Cor−TCPDA**), it is shown on one of the **TCPDA** acceptors as well, which indicates that the transition pathway is from **TCPDA** to **Per**. This TD-DFT result explains the relationship between λ_{em} and the ionization potential of **Per−TCPDA** from experiments that do not follow the theoretical prediction. The theoretical data agree with the SC-XRD results: i.e., a greater distorted degree of the PAH donor in the ground state led to an increase in the electron excitation energy of the structural transformation in the excited state. The **Per−TCPDA** cocrystal exhibits (Figure S8) a significant angle change (5.2° vs 2.2° and ∼0°) compared to the other two cocrystals (Figures S6 and S7). This D−A system shows the largest nonradiative transition, which may result in suppression of the long wavelength emission.

To gain insight into the determining factors of photophysical and photochemical properties, the absolute quantum yield (Φ) and average fluorescence lifetime (τ_{av}) of **TCPDA** and cocrystals were measured at room temperature (Table S6). Both **TCPDA** and cocrystals yielded negligibly weak emissions (Φ < 1%) under UV irradiation. The lifetimes were measured, and the corresponding emission decay curves are shown in Figures S23−S25. The τ_{av} values of cocrystals are in the range of ∼10 ns. These results indicate that the photoluminescence of each cocrystal is a fluorescence emission resulting from the excited electronic CT states of the cocrystals without other competing radiation processes and the PL state of cocrystals is a CT state (the lowest excited state, "CT 1 state"). Furthermore, the wide λ_{em} range of the cocrystals indicates that highly tunable D−A interactions could be achieved based on the twisted **TCPDA** component as a robust acceptor.

https://doi.org/10.1021/acsmaterialslett.5c00275
ACS Materials Lett. 2025, 7, 2246−2254

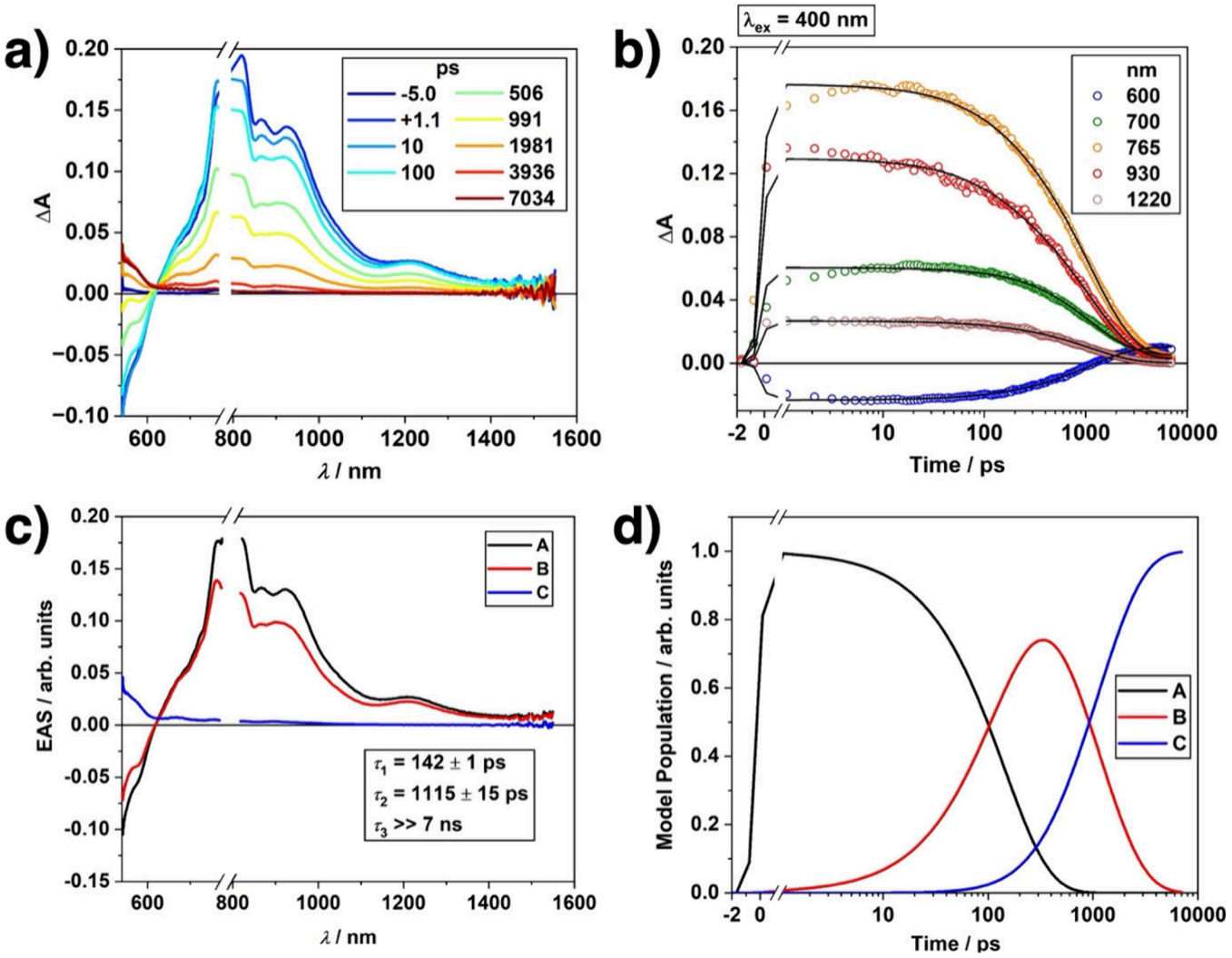

Figure 4. Transient absorption spectra of the TP−TCPDA cocrystal. (a) Combined fsTA and nsTA spectra of TP−TCPDA in THF at 298 K following a ∼150 fs, 400 nm (5 mJ/pulse) excitation. (b) Multiple-wavelength fits and time constants from the fsTA for TP−TCPDA (λ_{ex} = 400 nm). (c) Evolution-associated spectra for an A→B→C→ground state sequential decay model. (d) Population model kinetic profiles.

Light excitation induced electronic transitions between the ground CT (CT_0) state to the excited CT (CT*) states (Figure S26). Excitons in these excited CT_n states relax to the lowest CT_1 state via internal conversion (IC) or vibrational relaxation.[68,69] The femtosecond transient absorption (fsTA) spectrum of the **TP−TCPDA** cocrystal is shown in Figure 4a. Upon excitation, strong excited-state absorption features appear between ∼800 and 930 nm along with a strong peak in the NIR region, both of which were associated with $CT_n \leftarrow CT_0$ absorptions. The transient kinetics were analyzed globally (Figure 4b), and the all-time constants are listed in Figure 4c. The absorptions shifted subtly and decayed over the next several hundred picoseconds as the **TP−TCPDA** underwent modest structural changes to accommodate the CT excited state prior to decay. The first lifetime, $\tau_{A\rightarrow B}$, measured at 142 ± 1 ps, corresponds to the relaxation from the initially populated CT* state to the lowest-energy CT_1 state, most likely involving electronic relaxation and structural reorganization, rather than purely vibrational relaxation.[70] However, the subsequent lifetime, $\tau_{B\rightarrow C}$ = 1115 ± 15 ps, not only corresponds to decay of the CT state to the ground and ^{3}***TCPDA** states but also encompasses IC and radiative decay. This aligns with the energy gap law, which suggests that the strong nonradiative IC process predominates, resulting in a photothermal effect rather than the anticipated NIR emission for CT complexes with small band gaps (Figure 4d). Consequently, the NIR radiative decay yield was negligible, reinforcing our conclusions regarding the energy dissipation processes at play.[23,71]

Inspired by the long wavelength IR fluorescence emission spectrum, we explored the NIR-II two-photon fluorescence (2PF) performance of the cocrystals. Under the laser irradiation in NIR-I (870 nm) and NIR-II (1050, 1200, and 1300 nm) regions, fluorescence emission micrographs of TP−TCPDA cocrystals were collected (Figure 5a and Figure S27) in the red-color Vis region (650−750 nm) detection channel of a 2PF microscope, exhibiting a close correspondence with its fluorescence spectrum (λ_{ex} = 693 nm). With a scanning λ_{ex} of 700−1300 nm, the spectra (Figure 5b and Figure S28) showed that **TP−TCPDA** cocrystals are capable of emitting light at a shorter wavelength upon excitation at a longer wavelength. Similar emission spectra profiles were observed for **TP−TCPDA** regardless of one-photon absorption (1PA), or 2PA, indicating that their emission involves the

https://doi.org/10.1021/acsmaterialslett.5c00275
ACS Materials Lett. 2025, 7, 2246−2254

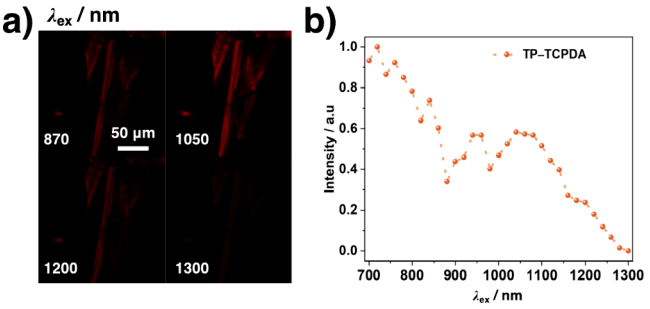

Figure 5. (a) Two-photon fluorescence (2PF) micrographs of TP−TCPDA cocrystal excited by λ_{ex} = 870, 1050, 1200, and 1300 nm, respectively. (b) Data plots of the upconversion fluorescence intensity dependent on λ_{ex}, which shows 2PF of TP−TCPDA. The excited laser power is set constantly at 2.7 mW.

same electronic state. In contrast, neither **Cor−TCPDA** nor **Per−TCPDA** cocrystals exhibit any 2PF in the NIR-II region.

The principle of the 2PF NIR-II imaging of **TP−TCPDA** was compared with that of its analogs **Cor−TCPDA** and **Per−TCPDA**. From the fingerprint (Figures S20−S22), the proportion of C atoms on the fused ring interacting with the outside world followed the trend of **TP** < **Per** < **Cor**, which correlated with the increasing area of PAHs and [$\pi\cdots\pi$] interaction. Both **TP** and **Cor** exhibited obvious hydrogen bonding with the O atoms in adjacent **TCPDA** components of surrounding molecules. In contrast, **Per** was the only one that had almost no hydrogen bonding with surrounding **TCPDA** in the **Per−TCPDA** (Figure S9, right) cocrystal. In addition, **TCPDA** units in **TP−TCPDA** (Figure S9, left) formed intralayer [C−H···Cl] hydrogen bonds. The stronger interlayer stacking induces active intramolecular vibrations, which dissipate the energy of the excited molecules, leading to fluorescence quenching. The cocrystal superstructure depended on the multiple noncovalent interactions, which were favorable to suppress the intramolecular vibrations and reduce the energy loss of the excited molecules, contributing to the realization of the efficient NIR emission. These results suggest that the weaker CT interaction and fine-tuning of the control of hydrogen bonds may be more helpful in achieving a two-photon response. The design of twisted components in cocrystals emerges as an alternative approach for the construction of NIR-absorbing materials.

In summary, we have developed a pseudoencapsulation strategy that was used to produce three D−A organic cocrystals in a rational way. Analyses of solid-state superstructures reveal that these cocrystals have the same stoichiometric ratio (D:A = 2:1) driven by CT interactions between the twisted acceptor and respective donors. The twisted **TCPDA** acceptor regulated the geometry of the donors, constructing well-aligned D−A stacking superstructures. Fluorescence emission spectra exhibited a maximum λ_{em} of up to 861 nm, while TA spectroscopic analysis showed that **TP−TCPDA** and **Cor−TCPDA** photoexcitations populate vibrationally hot CT states. There is a fast vibrational relaxation followed by a slower combination of IC (dominant) and emission (minor) to the ground state alongside ISC (moderate) to the triplet state. Benefiting from CT interactions and fine-tuning control of intralayer hydrogen bonds, the **TP−TCPDA** cocrystal with 2PA bands extends into the NIR-II region. Their readily tunable twisted acceptor with CT-based emissions of donors makes them promising candidates as potential luminophores. Importantly, D−A, [$\pi\cdots\pi$], and hydrogen bonding interactions play advantageous roles in reducing the fluorescence quenching, allowing for a high-efficiency NIR emission via forming the weak π-conjugated configuration and suppressing intramolecular vibrations. Overall, our investigation provides a deeper insight into the CT in twisted organic cocrystals and its related photophysics of the desired NIR emission. By applying the pseudoencapsulation strategy, we not only constitute twisted component-containing cocrystals that exhibit NIR 2PA and 2PF but also introduce a powerful tool for discovering the (super)structure−property relationship.

■ ASSOCIATED CONTENT

Supporting Information

The Supporting Information is available free of charge at https://pubs.acs.org/doi/10.1021/acsmaterialslett.5c00275.

Thermogravimetric analysis, optical spectra, DFT calculations, X-ray crystal data, two-photon microscopy, including Tables S1−S6 and Figures S1−S28 (PDF)

Accession Codes

Crystallographic data for cocrystals (CCDC 2333787−2333789).

■ AUTHOR INFORMATION

Corresponding Authors

Yuanning Feng − *Department of Chemistry and Biochemistry, The University of Oklahoma, Norman, Oklahoma 73019, United States*; orcid.org/0000-0002-8832-0767; Email: YF@ou.edu

Jian-Hua Jia − *Key Laboratory of Bioinorganic and Synthetic Chemistry of Ministry of Education, School of Chemistry, IGCME, GBRCE for Functional Molecular Engineering, Sun Yat-Sen University, Guangzhou, Guangdong 510006, China*; orcid.org/0000-0001-6342-2057; Email: jiajh3@mail.sysu.edu.cn

Authors

Tao Li − *Key Laboratory of Bioinorganic and Synthetic Chemistry of Ministry of Education, School of Chemistry, IGCME, GBRCE for Functional Molecular Engineering, Sun Yat-Sen University, Guangzhou, Guangdong 510006, China; Department of Chemistry and Biochemistry, The University of Oklahoma, Norman, Oklahoma 73019, United States*

Bai-Tong Liu − *Department of Chemistry, The University of Hong Kong, Hong Kong, SAR 999077, China*

Jia-Chuan Liu − *Key Laboratory of Bioinorganic and Synthetic Chemistry of Ministry of Education, School of Chemistry, IGCME, GBRCE for Functional Molecular Engineering, Sun Yat-Sen University, Guangzhou, Guangdong 510006, China*

Niharika Ashutosh Sule − *Department of Chemistry and Biochemistry, The University of Oklahoma, Norman, Oklahoma 73019, United States*

Jennifer T. Ou − *Department of Chemistry and Biochemistry, The University of Oklahoma, Norman, Oklahoma 73019, United States*

Jim Y. Huang − *Department of Chemistry and Biochemistry, The University of Oklahoma, Norman, Oklahoma 73019, United States*

Chenxin Ou − *Department of Chemistry and Biochemistry, The University of Oklahoma, Norman, Oklahoma 73019, United States*

https://doi.org/10.1021/acsmaterialslett.5c00275
ACS Materials Lett. 2025, 7, 2246−2254

Complete contact information is available at:
https://pubs.acs.org/10.1021/acsmaterialslett.5c00275

Author Contributions

T.L. and B.-T.L. contributed equally to this work. J.-H.J. provided funding for the experiments. Y.F. provided financial support for the HR and publishing expenses. T.L. conceived the idea, designed and executed the experiments, and wrote the initial draft of the manuscript. B.-T.L. analyzed the SC-XRD data and conducted two-photon microscopy measurements. J.-C.L. and T.L. conducted the DFT calculations. T.L., J.Y.H., and Y.F. edited the paper. T.L., B.T.-L., N.A.S., J.T.O., and Y.F. revised the manuscript and responded to the reviewers' comments. Y.F. and C.O. designed the schematic diagrams and the graphical abstract.

Notes

The authors declare no competing financial interest.

■ ACKNOWLEDGMENTS

Financial support was provided by the Junior Faculty Fellowship Program from the Research Council, Office of the Vice President for Research and Partnerships and the Office of the Provost at The University of Oklahoma as well as the National Natural Science Foundation of China (No. 22488101). The authors thank Professor Ryan M. Young at Northwestern University for his contribution to the data analysis of the TA spectra.

■ REFERENCES

(1) Dai, M.; Yang, Y. J.; Sarkar, S.; Kyo, H. N. Strategies to Convert Organic Fluorophores Into Red/Near-Infrared Emitting Analogues and their Utilization in Bioimaging Probes. *Chem. Soc. Rev.* **2023**, *52*, 6344−6358.

(2) Li, J.-K.; Zhang, M.-Y.; Zeng, L.; Huang, L.; Wang, X.-Y. NIR-Absorbing B,N-Heteroarene as Photosensitizer for High-Performance NIR-to-Blue Triplet-Triplet Annihilation Upconversion. *Angew. Chem., Int. Ed.* **2023**, *62*, No. e202303093.

(3) Wang, Z.; Zhu, C.-Y.; Yin, S.-Y.; Wei, Z.-W.; Zhang, J.-H.; Fan, Y.-N.; Jiang, J.-J.; Pan, M.; Su, C.-Y. A Metal-Organic Supramolecular Box as a Universal Reservoir of UV, WL, and NIR Light for Long-Persistent Luminescence. *Angew. Chem., Int. Ed.* **2019**, *58*, 3481−3485.

(4) Sun, S.; Ma, L.; Wang, J.; Ma, X.; Tian, H. Red-Light Excited Efficient Metal-Free Near-Infrared Room-Temperature Phosphorescent Films. *Natl. Sci. Rev.* **2022**, *9*, nwab085.

(5) Antaris, A. L.; Chen, H.; Cheng, K.; Sun, Y.; Hong, G.; Qu, C.; Diao, S.; Deng, Z.; Hu, X.; Zhang, B.; Zhang, X.; Yaghi, O. K.; Alamparambil, Z. R.; Hong, X.; Cheng, Z.; Dai, H. A Small-Molecule Dye for NIR-II Imaging. *Nat. Mater.* **2016**, *15*, 235−242.

(6) Sreejith, S.; Joseph, J.; Lin, M.; Menon, N. V.; Borah, P.; Ng, H. J.; Loong, Y. X.; Kang, Y.; Yu, W.-K.; Zhao, Y. Near-Infrared Squaraine Dye Encapsulated Micelles for in Vivo Fluorescence and Photoacoustic Bimodal Imaging. *ACS Nano* **2015**, *9*, 5695−5704.

(7) Wang, X. F.; Xiao, H.; Chen, P. Z.; Yang, Q. Z.; Chen, B.; Tung, C. H.; Chen, Y. Z.; Wu, L. Z. Pure Organic Room Temperature Phosphorescence from Excited Dimers in Self-Assembled Nanoparticles under Visible and Near-Infrared Irradiation in Water. *J. Am. Chem. Soc.* **2019**, *141*, 5045−5050.

(8) Lan, Z.; Lei, Y.; Chan, W. K. E.; Chen, S.; Luo, D.; Zhu, F. Near-Infrared and Visible Light Dual-Mode Organic Photodetectors. *Sci. Adv.* **2020**, *6*, No. eaaw8065.

(9) Minotto, A.; Haigh, P. A.; Łukasiewicz, Ł. G.; Lunedei, E.; Gryko, D. T.; Darwazeh, I.; Cacialli, F. Visible Light Communication with Efficient Far-Red/Near-Infrared Polymer Light-Emitting Diodes. *Light: Sci. Appl.* **2020**, *9*, 70.

(10) Tuong Ly, K.; Chen-Cheng, R.-W.; Lin, H.-W.; Shiau, Y.-J.; Liu, S.-H.; Chou, P.-T.; Tsao, C.-S.; Huang, Y.-C.; Chi, Y. Near-Infrared Organic Light-Emitting Diodes with Very High External Quantum Efficiency and Radiance. *Nat. Photonics* **2017**, *11*, 63−68.

(11) Yang, Y.; Hughes, R. P.; Aprahamian, I. Near-Infrared Light Acivated Azo-BF_2 Switches. *J. Am. Chem. Soc.* **2014**, *136*, 13190−13193.

(12) Wei, Y.-C.; Wang, S. F.; Hu, Y.; Liao, L.-S.; Chen, D.-G.; Chang, K.-H.; Wang, C.-W.; Liu, S.-H.; Chan, W.-H.; Liao, J.-L.; Hung, W.-Y.; Wang, T.-H.; Chen, P.-T.; Hsu, H.-F.; Chi, Y.; Chou, P.-T. Overcoming the Energy Gap Low in Near-Infrared OLEDs by Exciton-Vibration Decoupling. *Nat. Photonics.* **2020**, *14*, 570−577.

(13) Mu, J.; Xiao, M.; Shi, Y.; Geng, X.; Li, H.; Yin, Y.; Chen, X. The Chemistry of Organic Contrast Agents in the NIR-II Window. *Angew. Chem., Int. Ed.* **2022**, *61*, No. e202114722.

(14) Shi, W.-Q.; Zeng, L.; He, R.-L.; Han, X.-S.; Guan, Z.-J.; Zhou, M.; Wang, Q.-M. Near-Unity NIR Phosphorescent Quantum Yield from a Room-Temperature Solvated Metal Nanocluster. *Science* **2024**, *383*, 326−330.

(15) Chen, H.; Shi, X.; Lun, Y.; Xu, Y.; Lu, T.; Duan, Z.; Shao, M.; Sessler, J. L.; Yu, H.; Lei, C. 3,6-Carbazoylene Octaphyrin (1.0.0.0.1.0.0.0) and its Bis-BF_2 Complex. *J. Am. Chem. Soc.* **2022**, *144*, 8194−8203.

(16) Yan, D.; Xie, W.; Zhang, J.; Wang, L.; Wang, D.; Tang, B. Z. Donor/π-Bridge Manipulation for Constructing a Stable NIR-II Aggregation-Induced Emission Luminogen with Balanced Phototheranostic Performance. *Angew. Chem., Int. Ed.* **2021**, *60*, 26769−26776.

(17) Wan, H.; Yue, J.; Zhu, S.; Uno, T.; Zhang, X.; Yang, K.; Yu, K.; Hong, G.; Wang, J.; Li, L.; Ma, Z.; Gao, H.; Zhong, Y.; Su, J.; Antaris, A. L.; Xia, Y.; Luo, J.; Liang, Y.; Dai, H. A Bright Organic NIR-II Nanofluorophore for Three-Dimensional Imaging into Biological Tissues. *Nat. Commun.* **2018**, *9*, 1171.

(18) Jin, G.-Q.; Chau, C. V.; Arambula, J. F.; Gao, S.; Sessler, J. L.; Zhang, J.-L. Lanthanide Porphyrinoids as Molecular Theranostics. *Chem. Soc. Rev.* **2022**, *51*, 6177−6209.

(19) Padalkar, V. S.; Seki, S. Excited-State Intramolecular Proton-Transfer (ESIPT)-Inspired Solid State Emitters. *Chem. Soc. Rev.* **2016**, *45*, 169−202.

(20) Zampetti, A.; Minotto, A.; Cacialli, F. Near-Infrared (NIR) Organic Light-Emitting Diodes (OLEDs): Challenges and Opportunities. *Adv. Funct. Mater.* **2019**, *29*, 1807623.

(21) Yang, Q.; Hu, Z.; Zhu, S.; Ma, R.; Ma, H.; Ma, Z.; Wan, H.; Zhu, T.; Jiang, Z.; Liu, W.; Jiao, L.; Sun, H.; Liang, Y.; Dai, H. Donor Engineering for NIR-II Molecular Fluorophores with Enhanced Fluorescent Performance. *J. Am. Chem. Soc.* **2018**, *140*, 1715−1724.

(22) Zhao, L.; Ren, X.; Yan, X. Assembly Induced Super-Large Red-Shifted Absorption: The Burgeoning Field of Organic Near-Infrared Materials. *CCS Chem.* **2021**, *3*, 678−693.

(23) Zhuo, M.-P.; Yuan, Y.; Su, Y.; Chen, S.; Chen, Y.-T.; Feng, Z.-Q.; Qu, Y.-K.; Li, M.-D.; Li, Y.; Hu, B.-W.; Wang, X.-D.; Liao, L.-S. Segregated Array Tailoring Charge-Transfer Degree of Organic Cocrystal for the Efficient Near-Infrared Emission beyond 760 nm. *Adv. Mater.* **2022**, *34*, 2107169.

(24) Zhuo, M.-P.; Wang, X.-D.; Liao, L.-S. Recent Progress of Novel Organic Near-Infrared-Emitting Materials. *Small Sci.* **2022**, *2*, 2200029.

(25) Wu, J.; Shi, Z.; Zhu, L.; Li, J.; Han, X.; Xu, M.; Hao, S.; Fan, Y.; Shao, T.; Bai, H.; Peng, B.; Hu, W.; Liu, X.; Yao, C.; Li, L.; Huang, W. The Design and Bioimaging Applications of NIR Fluorescent Organic Dyes with High Brightness. *Adv. Opt. Mater.* **2022**, *10*, 2102514.

(26) Kim, H. M.; Cho, B. R. Small-Molecule Two-Photon Probes for Bioimaging Applications. *Chem. Rev.* **2015**, *115*, 5014−5055.

(27) Durr, N. J.; Larson, T.; Smith, D. K.; Korgel, B. A.; Sokolov, K.; Ben-Yakar, A. Two-Photon Luminescence Imaging of Cancer Cells Using Molecularly Targeted Gold Nanorods. *Nano Lett.* **2007**, *7*, 941−945.

(28) Zheng, Z.; Li, D.; Liu, Z.; Peng, H.-Q.; Sung, H. H. Y.; Kwok, R. T. K.; Williams, I. D.; Lam, J. W. Y.; Qian, J.; Tang, B. Z.

Aggregation-Induced Nonlinear Optical Effects of AIEgen Nanocrystals for Ultradeep in vivo Bioimaging. *Adv. Mater.* **2019**, *31*, 1904799.
(29) Sun, C.-L.; Li, J.; Wang, X.-Z.; Shen, R.; Liu, S.; Jiang, J.-Q.; Li, T.; Song, Q.-W.; Liao, Q.; Fu, H.-B.; Yao, J.-N.; Zhang, H.-L. Rational Design of Organic Probes for Turn-on Two-Photon Excited Fluorescence Imaging and Photodynamic Therapy. *Chem.* **2019**, *5*, 600−616.
(30) Zheng, Z.; Zhang, T.; Liu, H.; Chen, Y.; Kwok, R. T. K.; Ma, C.; Zhang, P.; Sung, H. H. Y.; Williams, I. D.; Lam, J. W. Y.; Wong, K. S.; Tang, B. Z. Bright Near-Infrared Aggregation-Induced Emission Luminogens with Strong Two-Photon Absorption, Excellent Organelle Specificity, and Efficient Photodynamic Therapy Potential. *ACS Nano* **2018**, *12*, 8145−8159.
(31) Wang, C.; Zhong, W.; Sun, X.; Guo, J.; Chen, Y.; Zhao, Y.; Han, J.; Zhao, Y. NIR-Activable Charge Transfer Agents for Synergistic Photoimmunotherapy. *Angew. Chem., Int. Ed.* **2025**, *64*, No. e202416828.
(32) Lim, A. J.; Littlefield, K. P.; Alkalani, Z.; Feng, Y. Synergistic Cancer Photoimmunotherapy by Harnessing Near Infrared-Activated Nanoparticles Containing Charge Transfer Complexes. *Angew. Chem., Int. Ed.* **2025**, *64*, No. e202423550.
(33) Cumpston, B. H.; Ananthavel, S. P.; Barlow, S.; Dyer, D. L.; Ehrlich, J. E.; Erskine, L. L.; Heikal, A. A.; Kuebler, S. M.; Lee, I. Y. S.; McCord-Maughon, D.; Qin, J.; Röckel, H.; Rumi, M.; Wu, X.-L.; Marder, S. R.; Perry, J. W. Two-Photon Polymerization Initiators for Three-Dimensional Optical Data Storage and Microfabrication. *Nature* **1999**, *398*, 51−54.
(34) Gan, Z.; Cao, Y.; Evans, R. A.; Gu, M. Three-Dimensional Deep Sub-Diffraction Optical Beam Lithography with 9 nm Feature Size. *Nat. Commun.* **2013**, *4*, 2061.
(35) Yu, J.; Cui, Y.; Wu, C.-D.; Yang, Y.; Chen, B.; Qian, G. Two-Photon Responsive Metal-Organic Framework. *J. Am. Chem. Soc.* **2015**, *137*, 4026−4029.
(36) Liang, W.; He, S.; Wu, S. Fluorescence Imaging in Second Near-Infrared Window: Developments, Challenges, and Opportunities. *Adv. NanoBiomed. Res.* **2022**, *2*, 2200087.
(37) Wang, Y.; Wu, H.; Li, P.; Chen, S.; Jones, L. O.; Mosquera, A.; Zhang, L.; Cai, K.; Chen, H.; Chen, X.-Y.; Stern, C. L.; Wasielewski, M. R.; Ratner, M. A.; Schatz, G. C.; Stoddart, J. F. Two-Photon Excited Deep-Red and Near-Infrared Emissive Organic Co-Crystals. *Nat. Commun.* **2020**, *11*, 4633.
(38) Sun, L.; Zhu, W.; Wang, W.; Yang, F.; Zhang, C.; Wang, S.; Zhang, X.; Li, R.; Dong, H.; Hu, W. Intermolecular Charge-Transfer Interactions Facilitate Two-Photon Absorption in Styrylpyridine-Tetracyanobenzene Cocrystals. *Angew. Chem., Int. Ed.* **2017**, *56*, 7831−7835.
(39) Yang, X.-G.; Zhai, Z.-M.; Lu, X.-M.; Ma, L.-F; Yan, D. Fast Crystallization-Deposition of Orderly Molecule Level Heterojunction Thin Films Showing Tunable Up-Conversion and Ultrahigh Photoelectric Response. *ACS Cent. Sci.* **2020**, *6*, 1169−1178.
(40) Zhang, J.; Xu, W.; Sheng, P.; Zhao, G.; Zhu, D. Organic Donor-Acceptor Complexes as Novel Organic Semiconductors. *Acc. Chem. Res.* **2017**, *50*, 1654−1662.
(41) Sun, L.; Zhu, W.; Zhang, X.; Li, L.; Dong, H.; Hu, W. Creating Organic Functional Materials beyond Chemical Bond Synthesis by Organic Cocrystal Engineering. *J. Am. Chem. Soc.* **2021**, *143*, 19243−19256.
(42) Geng, L.; Wang, K.; Sun, R.; Li, C.-T.; Li, X.-R.; Zhang, M.; Yu, M.-H.; Chang, Z.; Bu, X.-H. Donor-Acceptor Metal-Organic Frameworks Featuring Tunable Triplet States for Multistimulus Responsive Room-Temperature Charge Transfer Phosphorescence. *CCS Chem.* **2025**, *7*, 416−428.
(43) Yoo, H. J.; Kim, N.; Lee, H.; Kim, D.; Ow, L. T. C.; Nam, H.; Kim, C.; Lee, S. Y.; Lee, K.-Y.; Kim, D.; Han, S. S. Bespoke Metal Nanoparticle Synthesis at Room Temperature and Discovery of Chemical Knowledge on Nanoparticle Growth via Autonomous Experimentations. *Adv. Funct. Mater.* **2024**, *34*, 2470147.
(44) Xu, J.; Chen, W.; Li, S.; Chen, Q.; Wang, T.; Shi, Y.; Deng, S.; Li, M.; Wei, P.; Chen, Z. Organic Stoichiometric Cocrystals with a Subtle Balance of Charge-Transfer Degree and Molecular Stacking Towards High-Efficiency NIR Photothermal Conversion. *Chin. Chem. Lett.* **2024**, *35*, 109808.
(45) Chen, Y.-T.; Wen, X.; He, J.; Li, Z.; Zhu, S.; Chen, W.; Yu, J.; Guo, S.; Ni, S.; Chen, S.; Dang, L.; Li, M.-D. Boosting Near-Infrared Photothermal Conversion by Intermolecular Interactions in Isomeric Cocrystals. *ACS Appl. Mater. Interfaces.* **2022**, *14*, 28781−28791.
(46) Li, T.; Liu, J.-C.; Liu, E.-P; Liu, B.-T.; Wang, J.-Y.; Liao, P.-Y.; Jia, J.-H.; Feng, Y.; Tong, M.-L. NIR-II Photothermal Conversion and Imaging Based on a Cocrystal Containing Twisted Components. *Chem. Sci.* **2024**, *15*, 1692−1699.
(47) Yu, P.; Zhen, Y.; Dong, H.; Hu, W. Crystal Engineering of Organic Optoelectronic Materials. *Chem.* **2019**, *5*, 2814−2853.
(48) Guo, J.; Zeng, Y.; Zhen, Y.; Geng, H.; Wang, Z.; Yi, Y.; Dong, H.; Hu, W. Non-Equal Ratio Cocrystal Engineering to Improve Charge Transport Characteristics of Organic Semiconductors: A Case Study on Indolo[2,3-a]carbazole. *Angew. Chem., Int. Ed.* **2022**, *61*, No. e202202336.
(49) Tayi, A. S.; Shveyd, A. K.; Sue, A. C. H.; Szarko, J. M.; Rolczynski, B. S.; Cao, D.; Kennedy, T. J.; Sarjeant, A. A.; Stern, C. L.; Paxton, W. F.; Wu, W.; Dey, S. K.; Fahrenbach, A. C.; Guest, J. R.; Mohseni, H.; Chen, L. X.; Wang, K. L.; Stoddart, J. F.; Stupp, S. I. Room-Temperature Ferroelectricity in Supramolecular Networks of Charge-Transfer Complexes. *Nature* **2012**, *488*, 485−489.
(50) Li, S.; Lu, B.; Fang, X.; Yan, D. Manipulating Light-Induced Dynamic Macro-Movement and Static Photonic Properties within 1D Isostructural Hydrogen-Bonded Molecular Cocrystals. *Angew. Chem., Int. Ed.* **2020**, *59*, 22623−22630.
(51) Zhang, X.; De, J.; Liu, H.; Liao, Q.; Zhang, S.-T.; Zhou, C.; Fu, H.; Yang, B. Cis-Trans Isomerism Inducing Cocrystal Polymorphism with Thermally Activated Delayed Fluorescence and Two-Photon Absorption. *Adv. Opt. Mater.* **2022**, *10*, 2200286.
(52) Ning, G.-H.; Cui, P.; Sazanovich, I. V.; Pegg, J. T.; Zhu, Q.; Pang, Z.; Wei, R.-J.; Towrie, M.; Jelfs, K. E.; Little, M. A.; Cooper, A. I. Organic Cage Inclusion Crystals Exhibiting Guest-enhanced Multiphoton Harvesting. *Chem.* **2021**, *7*, 3157−3170.
(53) Sun, L.; Wang, Y.; Yang, F.; Zhang, X.; Hu, W. Cocrystal Engineering: A Collaborative Strategy toward Functional Materials. *Adv. Mater.* **2019**, *31*, 1902328.
(54) Chen, H.; Roy, I.; Myong, M. S.; Seale, J. S. W.; Cai, K.; Jiao, Y.; Liu, W.; Song, B.; Zhang, L.; Zhao, X.; Feng, Y.; Liu, R.; Young, R. M.; Wasielewski, M. R.; Stoddart, J. F. Triplet-Triplet Annihilation Upconversion in a Porphyrinic Molecular Container. *J. Am. Chem. Soc.* **2023**, *145*, 10061−10070.
(55) Ouyang, G.; Rühe, J.; Zhang, Y.; Lin, M.-J.; Liu, M.; Würthner, F. Intramolecular Energy and Solvent-Dependent Chirality Transfer within a BINOL-Perylene Hetero-Cyclophane. *Angew. Chem., Int. Ed.* **2022**, *61*, No. e202206706.
(56) Weh, M.; Rühe, J.; Herbert, B.; Krause, A.-M.; Würthner, F. Deracemization of Carbohelicenes by a Chiral Perylene Bisimide Cyclophane Template Catalyst. *Angew. Chem., Int. Ed.* **2021**, *60*, 15323−15327.
(57) Furukawa, H.; Cordova, K. E.; O'Keeffe, M.; Yaghi, O. M. The Chemistry and Applications of Metal-Organic Frameworks. *Science* **2013**, *341*, 1230444.
(58) Diercks, C. S.; Yaghi, O. M. The Atom, the Molecule, and the Covalent Organic Framework. *Science* **2017**, *355*, No. eaal1585.
(59) Lin, Z.-J; Mahammed, A. R.; Liu, T.-F.; Cao, R. Multifunctional Porous Hydrogen-Bonded Organic Frameworks: Current Status and Future Perspectives. *ACS Cent. Sci.* **2022**, *8*, 1589−1608.
(60) Little, M. A.; Cooper, A. I. The Chemistry of Porous Organic Molecular Materials. *Adv. Funct. Mater.* **2020**, *30*, 1909842.
(61) Liu, B.-T.; Gong, S.-H.; Jiang, X.-T.; Zhang, Y.; Wang, R.; Chen, Z.; Zhang, S.; Kirlikovali, K. O.; Liu, T.-F.; Farha, O. K.; Cao, R. A Solution Processible Single-Crystal Porous Organic Polymer. *Nat. Synth.* **2023**, *2*, 873−879.
(62) Etherington, M. K.; Franchello, F.; Gibson, J.; Northey, T.; Santos, J.; Ward, J. S.; Higginbotham, H. F.; Data, P.; Kurowska, A.; Dos Santos, P. L.; Graves, D. R.; Batsanov, A. S.; Dias, F. B.; Bryce, M.

https://doi.org/10.1021/acsmaterialslett.5c00275
ACS Materials Lett. 2025, 7, 2246−2254

R.; Penfold, T. J.; Monkman, A. P. Regio- and Conformational Isomerization Critical to Design of Efficient Thermally-Activated Delayed Fluorescence Emitters. *Nat. Commun.* **2017**, *8*, 14987.
(63) Shen, S.; Baryshnikov, G. V.; Xie, Q.; Wu, B.; Lv, M.; Sun, H.; Li, Z.; Ågren, H.; Chen, J.; Zhu, L. Making Multi-Twisted Luminophores Produce Persistent Room-Temperature Phosphorescence. *Chem. Sci.* **2023**, *14*, 970−978.
(64) Cao, H.; Gao, Y.; Wu, B.; Zhang, J.; Wang, L.; Wei, P.; Liu, L.; Zou, H.; Zhou, H.; Zheng, Z.; Tang, B. Z. Tuning Molecular Packing by Twisting Structure to Facilely Construct Highly Efficient Solid-State Fluorophores for Two-Photon Bioimaging and Photodynamic Therapy. *Adv. Funct. Mater.* **2024**, *34*, 2315692.
(65) Su, B.; Geng, S.; Xiao, Z.; Xia, Z. Highly Distorted Antimony(III) Chloride $[Sb_2Cl_8]^{2-}$ Dimers for Near-Infrared Luminescence up to 1070 nm. *Angew. Chem., Int. Ed.* **2022**, *61*, No. e202208881.
(66) Ono, T.; Sugimoto, M.; Hisaeda, Y. Multicomponent Molecular Puzzles for Photofunction Design: Emission Color Variation in Lewis Acid-Base Pair Crystals Coupled with Guest-to-Host Charge Transfer Excitation. *J. Am. Chem. Soc.* **2015**, *137*, 9519−9522.
(67) Zhang, D.-S.; Gao, Q.; Chang, Z.; Liu, X.-T.; Zhao, B.; Xuan, Z.-H.; Hu, T.-L.; Zhang, Y.-H.; Zhu, J.; Bu, X.-H. Rational Construction of Highly Tunable Donor-Acceptor Materials Based on a Crystalline Host-Guest Platform. *Adv. Mater.* **2018**, *30*, 1804715.
(68) Dimitriev, O. P. Dynamics of Excitons in Conjugated Molecules and Organic Semiconductor Systems. *Chem. Rev.* **2022**, *122*, 8487−8593.
(69) Chen, X.; Zhang, X.; Xiao, X.; Wang, Z.; Zhao, J. Recent Developments on Understanding Charge Transfer in Molecular Electron Donor-Acceptor Systems. *Angew. Chem., Int. Ed.* **2023**, *62*, No. e202216010.
(70) Imahori, H.; Kobori, Y.; Kaji, H. Manipulation of Charge-Transfer States by Molecular Design: Perspective from "Dynamic Exciton". *Acc. Chem. Res.* **2021**, *2*, 501−514.
(71) Zhang, H.-Y.; Zhang, M.; Zhuo, H.; Yang, H.-Y.; Han, B.; Zheng, Y.-H.; Wang, H.; Lin, H.; Tao, S.-L.; Zheng, C.-J.; Zhang, X.-H. Unraveling Non-Radiative Decay Channels of Exciplexes to Construct Efficient Red Emitters for Organic Light-Emitting Diodes. *Chem. Sci.* **2024**, *15*, 14651−14659.

https://doi.org/10.1021/acsmaterialslett.5c00275
ACS Materials Lett. 2025, 7, 2246−2254